IOP PUBLISHING PHYSICS IN MEDICINE AND BIOLOGY

Phys. Med. Biol. **52** (2007) 3201–3226 doi:10.1088/0031-9155/52/11/018

Improved *k–t* BLAST and *k–t* SENSE using FOCUSS

Hong Jung[1], **Jong Chul Ye**[1,3] **and Eung Yeop Kim**[2]

[1] Bio-Imaging & Signal Processing Lab., Korea Advanced Institute of Science & Technology (KAIST), 373-1 Guseong-Dong, Yuseong-Gu, Daejon 305-701, Korea
[2] Department of Radiology and Research Institute of Radiological Sciences, Yonsei University College of Medicine, Seoul, Korea

E-mail: jong.ye@kaist.ac.kr.

Received 18 October 2006, in final form 21 March 2007
Published 10 May 2007
Online at stacks.iop.org/PMB/52/3201

Abstract

The dynamic MR imaging of time-varying objects, such as beating hearts or brain hemodynamics, requires a significant reduction of the data acquisition time without sacrificing spatial resolution. The classical approaches for this goal include parallel imaging, temporal filtering and their combinations. Recently, model-based reconstruction methods called *k–t* BLAST and *k–t* SENSE have been proposed which largely overcome the drawbacks of the conventional dynamic imaging methods without *a priori* knowledge of the spectral support. Another recent approach called *k–t* SPARSE also does not require exact knowledge of the spectral support. However, unlike *k–t* BLAST/SENSE, *k–t* SPARSE employs the so-called compressed sensing (CS) theory rather than using training. The main contribution of this paper is a new theory and algorithm that unifies the abovementioned approaches while overcoming their drawbacks. Specifically, we show that the celebrated *k–t* BLAST/SENSE are the special cases of our algorithm, which is asymptotically optimal from the CS theory perspective. Experimental results show that the new algorithm can successfully reconstruct a high resolution cardiac sequence and functional MRI data even from severely limited *k–t* samples, without incurring aliasing artifacts often observed in conventional methods.

(Some figures in this article are in colour only in the electronic version)

1. Introduction

Dynamic MRI is a technique to monitor dynamic processes such as brain hemodynamics and cardiac motion. Fast imaging sequences, such as echo-planar imaging (EPI) (Stehling *et al* 1991) or balanced steady-state free precession (bSSFP), have been widely used in practice for

[3] Author to whom any correspondence should be addressed.

this purpose (Carr 1958, Plein *et al* 2001). EPI employs a series of bipolar readout gradients to generate a train of gradient echoes so that zigzag k-space trajectories can be sampled under the envelop of a free-induction decay (FID). Hence, EPI is commonly used for functional MR imaging. However, the use of EPI alone sacrifices the image quality to achieve high temporal resolution. The ultrafast sequence called balanced SSFP or TrueFISP is now a standard acquisition pulse sequence for cardiovascular MR due to its high blood signal-to-noise ratio (SNR) and blood–myocardium contrast-to-noise ratio (CNR) (Plein *et al* 2001, Lee 2005). However, for the left ventricular (LV) function study, 8–12 slices from the LV base to the apex with temporal resolution better than 60 ms are often necessary (Lee 2005). Therefore, even with an ultrafast sequence, such as bSSFP or TrueFISP, the total volume acquisition within a single breath-hold is still challenging (Lee 2005).

Parallel imaging methods can be used to improve the temporal resolution of dynamic MRI. For example, SMASH (SiMultaneous Acquisition of Spatial Harmonics) (Sodickwon and Manning 1997), SENSE (SENSitivity Encoding) (Pruessmann *et al* 1999), PILS (Partially Parallel Imaging with Localized Sensitivities) (Griswold *et al* 2000), and GRAPPA (GeneRalized Autocalibrating Partially Parallel Acquisitions) (Griswold *et al* 2002) reduce the scan time by skipping the phase encoding steps. In the reconstruction phase, SENSE restores the original images from a set of aliased images by solving the linear sensitivity equation, whereas SMASH and GRAPPA calculate the missing k-space data directly using coil sensitivity to avoid aliasing. In principle, the data acquisition time for parallel imaging can be reduced up to the number of RF coils.

The method called UNFOLD (UNaliasing by Fourier-encoding the Overlaps Using the temporal Dimension) (Madore *et al* 1999) is another method for fast data acquisition. More specifically, UNFOLD obtains the Fourier data in a k–t space in a sheared grid pattern, in which the phase encoding in k-space is shifted for every frame. This results in the repetition of the support region in x–f space, and the original image can be reconstructed using a spatio-temporal filter. Theoretically, the optimal UNFOLD design problem can be formulated as the spatio-temporal sampling problem in the k–t space under the so-called time sequential sampling (TSS) constraint (Aggarwal *et al* 2002). Willis and Bresler (1995) showed that a high temporal and spatial resolution with a multifold reduction in the acquisition rate can be achieved using a lattice sampling schedule as long as the spectral supports are known.

Researchers have tried to combine UNFOLD with parallel imaging for even faster scanning or reduced artifacts. For example, TSENSE (Kellman *et al* 2001) combines UNFOLD with SENSE in such a way that any residual artifacts are temporally frequency-shifted to the band edge and thus may be further suppressed by temporal low-pass filtering; whereas UNFOLD-SMASH (Tsao 2002) obtains the additional phase encoding lines using SMASH, after which images are reconstructed using UNFOLD. A generalization of the optimized time sequential sampling theory by (Willis and Bresler 1995) for the phase array coil data acquisition has recently been independently proposed by Sharif and Bresler (2006) and Kim *et al* (2006). The noticeable difference of the new methods from Willis and Bresler (1995) is that these methods allow aliasing in the x–f domain in designing a sampling lattice. The aliased x–f image is then converted into the final aliasing free x–f image by exploiting the coil sensitivities. In theory, the maximal achievable acceleration factor can be up to the parallel imaging acceleration factor multiplied by that of the optimized time sequential sampling. However, the main technical difficulties of these algorithms are that (1) the x–f supports are not usually band-limited and that (2) the exact knowledge of the x–f supports are difficult to obtain.

Recently, model-based approaches called k–t BLAST and k–t SENSE have been proposed which largely overcome the shortcomings of the existing algorithms (Tsao *et al* 2003, 2005,

Kozerke *et al* 2004, Hansen *et al* 2004). The *k–t* BLAST and *k–t* SENSE take advantage of *a priori* information about the x–f support obtained from the training data set in order to enhance the image resolution during data acquisition time. Unlike the other methods, *k–t* BLAST and *k–t* SENSE do not require precise knowledge of the spectral support. Furthermore, the signal does not need finite support. Even if the spectral supports overlap due to aliasing, *a priori* information from the training data can be used to remedy the aliasing artifacts. Significant quality improvements have been reported compared to the conventional methods. Furthermore, using regular lattice sampling patterns, fast implementation is possible.

Other interesting dynamic MR imaging approaches are closely related to the recent theory of the 'compressed sensing (CS)' in the signal processing community (Donoho 2006, Candes *et al* 2006a), for example, *k–t* SPARSE (Lustig *et al* 2006a). According to the compressed sensing theory, perfect reconstruction is possible, even from samples dramatically smaller than the Nyquist sampling limit, as long as the nonzero spectral support is sparse and the samples are obtained at random locations (Donoho 2006). Even if the signal is not sparse, we can still recover the significant features of the signals if the signals are compressible. Furthermore, optimal sparse solutions can be obtained using computationally feasible L_1 minimization algorithms, such as the basis pursuit, matching pursuit methods, etc, rather than resorting to computationally expensive combinatorial optimization algorithms (Donoho 2006, Candes *et al* 2006a). Hence, the compressed sensing theory has great potential to solve imaging problems. The *k–t* SPARSE successfully employed the compressed sensing theory for cardiac imaging applications by transforming the time-varying image using a wavelet transform along the spatial direction and the Fourier transform along the temporal direction (Lustig *et al* 2006a). The compressed sensing idea has been also used for the MR angiography problem as well (Lustig *et al* 2006b). However, the main drawback of *k–t* SPARSE is the computational burden. Furthermore, due to the total variational regularization used in (Lustig *et al* 2006a, 2006b), cartoon-like artifacts are often observed. Related regularization-based algorithms have been also presented to reduce the temporal aliasing artifacts using regularization techniques (Portniaguine *et al* 2003).

One of the main contributions of this paper is the new algorithm called *k–t* FOCUSS (*k–t* space FOCal Underdetermined System Solver (FOCUSS)) that unifies the abovementioned approaches while overcoming their drawbacks. We show that our *k–t* FOCUSS is asymptotically optimal from a compressed sensing perspective and the celebrated *k–t* BLAST and *k–t* SENSE are the special cases of *k–t* FOCUSS.

The basis of *k–t* FOCUSS is another important class of sparse reconstruction algorithm called the FOCal Underdetermined System Solver (FOCUSS) (Gorodnitsky *et al* 1995, Gorodnitsky and Rao 1997, Kreutz-Delgado *et al* 2003). FOCUSS was originally designed to obtain sparse solutions by successively solving quadratic optimization problems and has been successfully used for EEG source localization (Gorodnitsky *et al* 1995, Gorodnitsky and Rao 1997). More specifically, FOCUSS starts by finding a low-resolution estimate of a sparse signal, and then this solution is pruned to a sparse signal representation. The pruning process is implemented by scaling the entries of the current solution by those of the solutions of previous iterations. Hence, once some entries of the previous solution become zero, these entries are fixed to zero values. As a consequence, we can obtain a sparser solution with more iterations. During the pruning process, the entries corresponding to the zero values on the original spectral support converge to zero. Hence, one of the important requirements of FOCUSS is the existence of a reasonable low-resolution initial estimate which provides the necessary extra constraint to resolve the non-uniqueness of the problem.

FOCUSS is a nice fit to the dynamic MRI. First, the training data or interleaved low-frequency *k–t* samples can provide the low-resolution initial estimate essential for the

convergence of FOCUSS. Second, FOCUSS incorporates the sparseness as a soft-constraint, whereas the conventional basis pursuit or orthogonal matching pursuit impose the constraint as a hard-constraint. The hard sparseness constraint may be not suitable for dynamic MRI since the abrupt changes of the image values introduce visually annoying high-frequency artifacts as reported in *k–t* SPARSE, especially when combined with total variation regularization (Lustig *et al* 2006a). The reconstruction image using FOCUSS, however, does not exhibit these behaviors since the nonzero image values are gradually suppressed. Third, FOCUSS can be very easily implemented in a computationally efficient manner using successive quadratic optimization. This is quite a big advantage over the other sparse optimization algorithms, such as basis pursuit or matching pursuit approaches. Finally, FOCUSS asymptotically achieves the optimal solution from the compressed sensing theory point of view. Experimental results demonstrate very quick convergence of the *k–t* FOCUSS to accurate solutions, even from highly sparse *k*-space samples.

This paper is organized as follows. Section 2 provides a detailed discussion of *k–t* FOCUSS. In section 3, the implementation issues of *k–t* FOCUSS are discussed. Our experimental results and discussion are presented in sections 4 and 5, respectively. Conclusions are given in section 6.

2. Theory

2.1. Problem formulation

Consider the Cartesian trajectory. The readout direction is along the k_y axis, and k_x denotes the phase encoding direction. The samples along the readout direction are fully sampled within T_R. Let $\sigma(x,t)$ denote the unknown image content (e.g., proton density, T1/T2 weighted image, etc) on x at time instance t. Then, the k-space measurement $\upsilon(k,t)$ at time t is given by

$$\upsilon(k,t) = \int \sigma(x,t)\, \mathrm{e}^{-\mathrm{j}2\pi kx}\, \mathrm{d}x = \iint \rho(x,f)\, \mathrm{e}^{-\mathrm{j}2\pi(kx+ft)}\, \mathrm{d}x\, \mathrm{d}f, \tag{1}$$

where $\rho(x,f)$ denotes the 2D spectral support in the x–f domain, and we use the following Fourier transform along the temporal direction:

$$\sigma(x,t) = \int \rho(x,f)\, \mathrm{e}^{-\mathrm{j}2\pi ft}\, \mathrm{d}f. \tag{2}$$

Let $\rho[n_x, n_f]$ denote the discretized (x,f)-image on $x = n_x\Delta x, n_x = 1,2,\ldots,N_x$ and $f = n_f\Delta f, n_f = 1,2,\ldots,N_f$, where Δx and Δf denote the sampling steps for x and f, respectively. Then, the k-space measurement $\upsilon[n_k, n_t]$ at the k-space location $k = n_k\Delta k, n_k = 1,\ldots,N_k$ and the time instance $t = n_t\Delta t, n_t = 1,\ldots,N_t$ can be approximated by the 2D discrete Fourier transform:

$$\upsilon[n_k,n_t] = \Delta x\Delta f \sum_{n_x=1}^{N_x}\sum_{n_f=1}^{N_f} \rho[n_x,n_f]\exp(-\mathrm{j}2\pi(n_k n_x\Delta k\Delta x + n_f n_t\Delta f\Delta t)). \tag{3}$$

According to the Nyquist sampling limit theory, to obtain an aliasing free image, the interval Δk on k-space should be $\Delta k \leqslant 1/(N_x\Delta x)$. In the same way, to reconstruct a time-varying image without temporal aliasing, we need $\Delta t \leqslant 1/(N_f\Delta f)$. Hence, at the Nyquist sampling rate, we have

$$\upsilon[n_k,n_t] = \frac{1}{\Delta k\Delta t N_x N_f}\sum_{n_x=1}^{N_x}\sum_{n_f=1}^{N_f} \rho[n_x,n_f]\exp(-j2\pi(n_k n_x/N_x + n_f n_t/N_f)). \tag{4}$$

In matrix form, equation (4) can be represented by

$$\upsilon = \mathbf{F}\rho, \tag{5}$$

where υ and ρ denote the stacked *k–t* space measurement vectors and the *x–f* image, respectively, and $\mathbf{F}$ denotes the 2D Fourier transform along the *x–f* direction. Here, it is important to note that the temporal Fourier transform equation (2) corresponds to a sparsifying operator of periodic motions, such as cardiac motion since the corresponding spectrum is the line spectrum from the Fourier series rather than the continuous spectrum. For general motions, there may exist more efficient transform to sparsify the signal, which will be discussed later.

Our main goal is to reduce the number of samples in the *k–t* space without sacrificing *x–f* image quality by taking advantage of the sparsity of *x–f* support. Here, recent theory of the compressed sensing (Donoho 2006, Candes *et al* 2006a, 2006b, Haupt and Nowak 2006, Candes and Tao 2005) can be applied. The compressed sensing theory tells us that the *perfect* reconstruction of ρ is possible from the *noiseless k–t* space samples that are dramatically smaller than the Nyquist sampling limit as long as the nonzero support of ρ is sparse and the *k–t* samples are obtained at random. More specifically, if ρ is nonzero at the *unknown M* locations, then the number of required *k–t* space measurement, K, can be dramatically smaller than the *x–f* domain pixel number, $N = N_x N_f$, and it is possible to design $K = O(M \log(N))$ number of measurements to obtain the perfect reconstruction of ρ with overwhelming probability by solving a L_1 minimization problem[4]. Second, if $K = O(M \log^6(N))$ discrete measurements in *k–t* space are *noisy* and their magnitudes are upper-bounded by the input noise power ϵ, then with overwhelming probability the reconstruction error is still upper bounded by ϵ multiplied with a finite constant. This concept can be effectively applied to dynamic MR imaging since only limited frequency components have significant values on *x–f* support of a dynamic sequence. Hence, we can expect the *graceful degradation* of the reconstruction image quality if the compressed sensing approach is applied for dynamic MR imaging problems.

Perhaps the most important implication of the compressed sensing theory is that the optimal sparse solution satisfying the abovementioned properties can be obtained by solving the L_1 minimization (Donoho 2006, Candes *et al* 2006a). More specifically, the optimal dynamic MR imaging problem from the compressed sensing perspective can be stated as follows:

$$\begin{aligned} &\text{minimize } \|\rho\|_1 \\ &\text{subject to } \|\upsilon - \mathbf{F}\rho\|_2 \leqslant \epsilon \end{aligned} \tag{6}$$

where $\|\cdot\|_1$ and $\|\cdot\|_2$ denote the L_1 and L_2 norm, respectively, and ϵ denotes the noise level.

2.2. Derivation of k–t FOCUSS

As explained before, the idea of compressed sensing is not new in the MR community. The *k–t* SPARSE (Lustig *et al* 2006a) successfully employed the compressed sensing theory for cardiac imaging applications by transforming the time-varying image using a wavelet transform along the spatial direction and the Fourier transform along the temporal direction. However, our compressed sensing approach is very different from (Lustig *et al* 2006a) and is much closer to *k–t* BLAST and *k–t* SENSE. This is because the basis of our approach is another type of sparse reconstruction method called the FOCal Underdetermined System Solver (FOCUSS) (Gorodnitsky *et al* 1995, Gorodnitsky and Rao 1997, Kreutz-Delgado *et al* 2003).

[4] The $O(\cdot)$ denotes the 'big O' notation to describe an asymptotic upper bound.

FOCUSS is an algorithm designed to obtain the sparse solutions to the underdetermined linear inverse problem given by (Gorodnitsky and Rao 1997, Kreutz-Delgado *et al* 2003)

$$\boldsymbol{\upsilon} = \mathbf{F}\boldsymbol{\rho}. \tag{7}$$

The solution of equation (7) is not unique; hence, the minimum norm solution is the most widely accepted. The minimum solution, however, does not provide a sparse reconstruction and has the tendency to smooth out the energy (Gorodnitsky and Rao 1997, Kreutz-Delgado *et al* 2003). Now, let us consider the following optimization problem:

$$\text{find } \boldsymbol{\rho} = \mathbf{W}\mathbf{q} \tag{8}$$

where $\boldsymbol{\rho}$ is an unknown x–f support, $\mathbf{W}$ is a weighting matrix, and $\mathbf{q}$ is a solution of the following constrained minimization problem:

$$\min \|\mathbf{q}\|_2, \qquad \text{subject to } \|\boldsymbol{\upsilon} - \mathbf{F}\mathbf{W}\mathbf{q}\|_2 \leqslant \epsilon. \tag{9}$$

The constrained optimization problem can be converted into the un-constrained optimization problem using the Lagrangian multiplier, providing a cost function:

$$C(\mathbf{q}) = \|\boldsymbol{\upsilon} - \mathbf{F}\mathbf{W}\mathbf{q}\|_2^2 + \lambda\|\mathbf{q}\|_2^2 \tag{10}$$

where λ denotes the appropriate Lagrangian parameter. The optimal solution minimizing equation (10) is then given by

$$\begin{aligned}\boldsymbol{\rho} &= \mathbf{W}\mathbf{q} \\ &= \boldsymbol{\Theta}\mathbf{F}^H\left(\mathbf{F}\boldsymbol{\Theta}\mathbf{F}^H + \lambda\mathbf{I}\right)^{-1}\boldsymbol{\upsilon}\end{aligned} \tag{11}$$

where $\boldsymbol{\Theta} = \mathbf{W}\mathbf{W}^H$. In a slightly different formulation, $\boldsymbol{\rho}$ is initialized with nonzero values $\bar{\boldsymbol{\rho}}$. In this case, the cost function equation (10) can be modified into the following form:

$$C(\mathbf{q}) = \|\boldsymbol{\upsilon} - \mathbf{F}\bar{\boldsymbol{\rho}} - \mathbf{F}\mathbf{W}\mathbf{q}\|_2^2 + \lambda\|\mathbf{q}\|_2^2 \tag{12}$$

where $\boldsymbol{\rho} = \bar{\boldsymbol{\rho}} + \mathbf{W}\mathbf{q}$, and the optimal solution is then given by

$$\boldsymbol{\rho} = \bar{\boldsymbol{\rho}} + \boldsymbol{\Theta}\mathbf{F}^H(\mathbf{F}\boldsymbol{\Theta}\mathbf{F}^H + \lambda\mathbf{I})^{-1}(\boldsymbol{\upsilon} - \mathbf{F}\bar{\boldsymbol{\rho}}). \tag{13}$$

The novelty of the FOCUSS algorithm comes from the fact that the weighting matrix $\mathbf{W}$ can be continuously updated using the previous solution (hence, $\boldsymbol{\Theta} = \mathbf{W}\mathbf{W}^H$ is updated accordingly). More specifically, if the $(n-1)$th iteration of the image estimate is given by

$$\boldsymbol{\rho}_{n-1} = [\rho_{n-1}(1), \rho_{n-1}(2), \ldots, \rho_{n-1}(N)]^T, \tag{14}$$

where N is the total number of data on x–f space, then the nth iteration of FOCUSS can be calculated by the following procedure (Kreutz-Delgado *et al* 2003).

(i) Compute the weighting matrix $\mathbf{W}_n$:

$$\mathbf{W}_n = \begin{pmatrix} |\rho_{n-1}(1)|^p & 0 & \cdots & 0 \\ 0 & |\rho_{n-1}(2)|^p & \cdots & 0 \\ \vdots & \vdots & \ddots & \vdots \\ 0 & 0 & \cdots & |\rho_{n-1}(N)|^p \end{pmatrix}, \qquad 1/2 \leqslant p \leqslant 1. \tag{15}$$

(ii) Compute $\boldsymbol{\Theta}_n = \mathbf{W}_n\mathbf{W}_n^H$.

(iii) Compute the nth FOCUSS estimate:

$$\boldsymbol{\rho}_n = \boldsymbol{\Theta}_n\mathbf{F}^H(\mathbf{F}\boldsymbol{\Theta}_n\mathbf{F}^H + \lambda\mathbf{I})^{-1}\boldsymbol{\upsilon}, \tag{16}$$

or, in another form

$$\boldsymbol{\rho}_n = \bar{\boldsymbol{\rho}} + \boldsymbol{\Theta}_n\mathbf{F}^H(\mathbf{F}\boldsymbol{\Theta}_n\mathbf{F}^H + \lambda\mathbf{I})^{-1}(\boldsymbol{\upsilon} - \mathbf{F}\bar{\boldsymbol{\rho}}). \tag{17}$$

(iv) If it converges, stop. Otherwise, increase n and go to step 1.

In order to understand why FOCUSS can provide a sparse solution, consider the nth FOCUSS estimate of the weighting matrix, $\mathbf{W}_n$. Then, equations (8) and (9) can be equivalently represented by

$$\min \left\| \mathbf{W}_n^{-1} \boldsymbol{\rho} \right\|_2^2, \qquad \text{subject to } \|\boldsymbol{\upsilon} - \mathbf{F}\boldsymbol{\rho}\|_2 \leqslant \epsilon. \tag{18}$$

Now we set $p = 0.5$ for equation (15). Then, we have the following asymptotic relation:

$$\begin{aligned} \left\| \mathbf{W}_n^{-1} \boldsymbol{\rho} \right\|_2^2 &= \boldsymbol{\rho}^H \mathbf{W}_n^{-H} \mathbf{W}_n^{-1} \boldsymbol{\rho} \\ &= \boldsymbol{\rho}^H \begin{pmatrix} |\rho_{n-1}(1)|^{-1} & 0 & \cdots & 0 \\ 0 & |\rho_{n-1}(2)|^{-1} & \cdots & 0 \\ \vdots & \vdots & \ddots & \vdots \\ 0 & 0 & \cdots & |\rho_{n-1}(N)|^{-1} \end{pmatrix} \boldsymbol{\rho} \\ &\sim \sum_{i=1}^{N} |\rho_{n-1}(i)| \quad \text{as } n \to \infty \\ &= \|\boldsymbol{\rho}\|_1 \end{aligned} \tag{19}$$

where $\sim$ implies the asymptotic equality as $n \to \infty$. This implies that the FOCUSS solution is asymptotically equivalent to the L_1 minimization solution when p is set to 0.5. At this time, L_1 is defined as the sum of the absolute values of the whole data. Since the L_1 minimization is the preferred optimization method for compressed sensing (Donoho 2006), the FOCUSS solution will asymptotically converge to the optimal solution from compressed sensing perspective by setting $p = 0.5$. Furthermore, according to (Gorodnitsky and Rao 1997), for $0.5 \leqslant p < 1$, the FOCUSS provides sparse solutions.

In summary, FOCUSS starts by finding a low-resolution estimate of the $\rho(x, f)$ to initialize the $\mathbf{W}_n$ matrix at $n = 0$, and this solution is *pruned* to a sparse signal representation. The pruning process is implemented by scaling the entries of the current solution by those of the solutions of previous iterations (Gorodnitsky and Rao 1997). Therefore, a good initial estimate of $\rho(x, f)$ is an important factor to guarantee the performance of the algorithm. In our implementation of *k–t* FOCUSS for dynamic MRI, we employ the random sampling pattern with more samples around the low-frequency region. Hence, the initial estimate can be easily obtained from the zero-padded direct Fourier inversion result without additional training data. Of course, an additional training set could be also used for the initial estimate of $\mathbf{W}_0$.

Recall that the *k–t* BLAST algorithm is given by Tsao *et al* (2003)

$$\boldsymbol{\rho}_1 = \bar{\boldsymbol{\rho}} + \boldsymbol{\Theta}_0 \mathbf{F}^H (\mathbf{F}\boldsymbol{\Theta}_0 \mathbf{F}^H + \lambda \mathbf{I})^{-1} (\boldsymbol{\upsilon} - \mathbf{F}\bar{\boldsymbol{\rho}}) \tag{20}$$

where $\boldsymbol{\Theta}_0$ is the diagonal covariance matrix obtained from the training data set and $\bar{\boldsymbol{\rho}}$ corresponds to the DC component (i.e. $f = 0$) in the x–f image. Comparing equation (20) with equation (17), we find that conventional *k–t* BLAST is indeed the first iteration of our *k–t* FOCUSS algorithm when the p value of equation (15) is set to 1 and $\bar{\boldsymbol{\rho}}$ is initialized using the temporal average (DC) values. Other advantages of our algorithm over *k–t* BLAST are summarized as follows.

(i) Our *k–t* FOCUSS is asymptotically optimal from the compressed sensing perspective. However, *k–t* BLAST does not minimize the L_1 norm; hence, it is not optimal from the compressed sensing perspective.

(ii) Instead of using the $p = 1$ value for the diagonal matrix $\boldsymbol{\Theta}_0$ as in *k–t* BLAST, our *k–t* FOCUSS can choose any values between 0.5 and 1. It turns out that $p = 0.5$ is usually the best choice that guarantees the stability and improved reconstruction quality.

2.3. k–t FOCUSS for parallel imaging

The extension of *k–t* FOCUSS to parallel imaging is quite straightforward. Recall that the measurement from a parallel coil is given by the 2D Fourier relationship:

$$\upsilon[n_k, n_t] = \frac{1}{\Delta k \Delta t N_x N_f} \sum_{n_x=1}^{N_x} \sum_{n_f=1}^{N_f} s_i[n_x]\rho[n_x, n_f] \exp(-\mathrm{j}2\pi(n_k n_x/N_x + n_f n_t/N_f)), \quad i = 1, \ldots, N_c, \tag{21}$$

where $s_i[n_x]$ denotes the ith coil sensitivity at $x = n_x \Delta x$ and N_c is the number of coils. In matrix form, equation (21) can be represented by

$$\boldsymbol{\upsilon}_i = \mathbf{F}\mathbf{S}_i\boldsymbol{\rho} \tag{22}$$

where $\mathbf{S}_i$ denotes the diagonal matrix composed of the ith sensitivity $s_i[n_x]$. Then, the cost function of the nth FOCUSS iteration becomes

$$C(\mathbf{q}) = \|\widehat{\boldsymbol{\upsilon}} - \widehat{\mathbf{F}}\mathbf{W}_n\mathbf{q}\|_2^2 + \lambda\|\mathbf{q}\|_2^2 \tag{23}$$

where $\widehat{\mathbf{F}}$ and $\widehat{\boldsymbol{\upsilon}}$ are given by

$$\widehat{\boldsymbol{\upsilon}} = \begin{bmatrix} \boldsymbol{\upsilon}_1 \\ \vdots \\ \boldsymbol{\upsilon}_{N_c} \end{bmatrix}, \qquad \widehat{\mathbf{F}} = \begin{bmatrix} \mathbf{F}\mathbf{S}_1 \\ \vdots \\ \mathbf{F}\mathbf{S}_{N_c} \end{bmatrix}. \tag{24}$$

Then, the optimal nth *k–t* FOCUSS update is given by

$$\boldsymbol{\rho}_n = \boldsymbol{\Theta}_n\widehat{\mathbf{F}}^H(\widehat{\mathbf{F}}\boldsymbol{\Theta}_n\widehat{\mathbf{F}}^H + \lambda\mathbf{I})^{-1}\widehat{\boldsymbol{\upsilon}} \tag{25}$$

where $\boldsymbol{\Theta}_n = \mathbf{W}_n\mathbf{W}_n^H$. Furthermore, if we initialize $\boldsymbol{\rho}$ with $\bar{\boldsymbol{\rho}}$, we have

$$\boldsymbol{\rho}_n = \bar{\boldsymbol{\rho}} + \boldsymbol{\Theta}_n\widehat{\mathbf{F}}^H(\widehat{\mathbf{F}}\boldsymbol{\Theta}_n\widehat{\mathbf{F}}^H + \lambda\mathbf{I})^{-1}(\widehat{\boldsymbol{\upsilon}} - \widehat{\mathbf{F}}\bar{\boldsymbol{\rho}}). \tag{26}$$

Again, the first iteration of equation (26) corresponds to *k–t* SENSE.

A slightly different, but computationally more efficient implementation of the *k–t* FOCUSS for parallel imaging can be obtained by separately applying *k–t* FOCUSS for each coil. More specifically, the algorithm is given by

(i) for each coil measurements $\boldsymbol{\upsilon}_i$, apply *k–t* FOCUSS to obtain the ith estimate $\hat{\mathbf{y}}_i = \mathbf{S}_i\hat{\boldsymbol{\rho}}$, where $i = 1, \ldots, N_c$,
(ii) from $\hat{\mathbf{y}}_i$, $i = 1, \ldots, N_c$, find the least-square estimate $\hat{\boldsymbol{\rho}}$:

$$\hat{\boldsymbol{\rho}} = \left(\sum_{i=1}^{N_c} \mathbf{S}_i\mathbf{S}_i^H\right)^{-1} \left(\sum_{i=1}^{N_c} \mathbf{S}_i^H\hat{\mathbf{y}}_i\right). \tag{27}$$

2.4. k–t FOCUSS using KLT/PCA

Even though our *k–t* FOCUSS has been developed using the temporal Fourier transform given in equation (2), a more general transform could be employed. The temporal Fourier transform is effective in sparsifying the signal when the image follows the periodic motion. However, for the objects with more general motion, other transforms may be more efficient in sparsifying the signal.

In the image and signal processing literature, an important transform for data compression is the Karhunen–Loeve transform (KLT), or the principle component analysis (PCA) (Poor

1994). Unlike the Fourier transform, the KLT/PCA is a data dependent transform. More specifically, let $\boldsymbol{\sigma}_x$ denote the discretized time-varying proton density at x as follows:

$$\boldsymbol{\sigma}_x = [\sigma(x, \Delta t) \quad \sigma(x, 2\Delta t) \cdots \sigma(x, N_t \Delta t)]^T \in \mathbf{C}^{N_t}. \tag{28}$$

Then, the covariance matrix $\mathbf{C}_x$ of $\boldsymbol{\sigma}_x$ can be expanded as follows:

$$\mathbf{C}_x = \sum_{k=1}^{N_t} \lambda_k \boldsymbol{\psi}_k \boldsymbol{\psi}_k^H \tag{29}$$

where $\{\lambda_k\}_{k=1}^{N_t}$ and $\{\boldsymbol{\psi}_k\}_{k=1}^{N_t}$ are the eigenvalues and the corresponding orthonormal eigenvectors (or principle components) of $\mathbf{C}_x$ (Poor 1994). Using equation (29), we can create the following expansion (Poor 1994):

$$\boldsymbol{\sigma}_x = \sum_{k=1}^{N_t} \rho_k^x \boldsymbol{\psi}_k, \tag{30}$$

for some expansion coefficients $\boldsymbol{\rho}^x = \left\{\rho_k^x\right\}_{k=1}^{N_t}$. It is well known that the KLT/PCA is the optimal energy compaction transform and that most of the energy is compacted in a small number of expansion coefficients (Poor 1994), which is an ideal property from the compressed sensing perspective.

Note that the principle components $\{\boldsymbol{\psi}_k\}_{k=1}^{N_t}$ in equation (30) are data dependent; hence, they are, in fact, varying with respect to the specific x position. However, estimating autocovariance for each x position is a very underdetermined problem due to the limited number of measurements. Hence, assuming that the motion of the moving parts is about the same for all x position, we can estimate the autocovariance function using measurements from all x. More specifically, in our *k–t* FOCUSS implementation, the low-resolution initial image can be easily obtained from training or interleaved low-frequency k-space samples. This information is used to estimate the covariance matrix $\mathbf{C}_x$. Then, the principle component $\{\boldsymbol{\psi}_k\}_{k=1}^{N_t}$ can be readily obtained using eigen-decomposition. It is important to note that even though principal components are obtained from low-spatial-resolution images, the temporal changes are not smoothed at all because we use fully sampled data along the temporal direction within limited low-spatial-frequency k-space in order to obtain full set of principal components. Therefore, the KLT/PCA keeps any high-temporal-frequency information.

After obtaining the expansion (30), the remaining part of our *k–t* FOCUSS algorithm is exactly the same as the temporal Fourier transform. More specifically, the unknown image vector to reconstruct is the KLT coefficients given by

$$\boldsymbol{\rho} = [\boldsymbol{\rho}^{\Delta x} \quad \boldsymbol{\rho}^{2\Delta x} \cdots \boldsymbol{\rho}^{N_x \Delta x}]^T \in \mathbb{C}^{N_x N_t \times 1}, \tag{31}$$

and the mapping $\mathbf{F}$ of equation (7) is given by the composite mapping of 1D DFT matrix with the eigenvector basis from KLT/PCA. Hence, we will not elaborate on the details of the implementation to avoid any duplicated explanation. In section 4, we will show that the KL transform is very effective for functional MRI analysis.

3. Implementation issues

In (Hansen *et al* 2004), the influence of the training set quality in the *k–t* BLAST was discussed in detail. The key observation was that the training set needs not produce a high-resolution covariance matrix estimate, and a low-resolution estimate is sufficient. Such observations in (Hansen *et al* 2004) can be easily explained from a FOCUSS point of view. Our previous

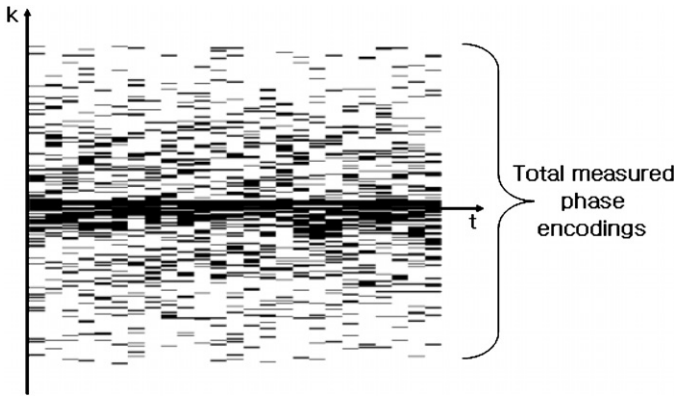

Figure 1. Gaussian random sampling pattern.

analysis showed that $\boldsymbol{\Theta}$ in k–t BLAST comes from the reweighted norm concept in FOCUSS rather than the covariance matrix. Since FOCUSS is a pruning algorithm that prunes a low-resolution image to a sparse image by reweighting the image using the previous reconstruction results, we do not need a high-resolution initial estimate of an x–f image.

Figure 1 illustrates an example of the k–t sampling pattern used in our paper. We generated samples according to a random distribution since the basic assumption of the compressed sensing is the use of a random sampling pattern. In order to obtain a low-resolution initial estimate without an additional training phase, a zero mean Gaussian distribution is used to generate a random sampling pattern with more frequent k-space samples at the spatial low-frequency regions.

The whole flow chart of our k–t FOCUSS algorithm is illustrated in figure 2. Here, the temporal average contribution is first subtracted from k–t samples, which are then converted to the x–f domain using the Fourier transform. The weighting matrix $\mathbf{W}$ at the first iteration is then obtained from the low-resolution initial estimate of the x–f support using equation (15). In principle, any power factor between $0.5 \leqslant p \leqslant 1$ could be used for equation (15). However, extensive simulation shows that the solution for $p = 1$ is too sparse, and $p < 0.5$ does not effectively remove the aliasing pattern from the random sampling pattern. Hence, the choice of $p = 0.5$ seems to be optimal in many applications. After the weighting matrix is constructed, a FOCUSS iteration step is performed. The newly calculated FOCUSS estimate of the x–f support is then again used to recalculate the $\mathbf{W}$ matrix. These steps are successively applied to obtain consecutive k–t FOCUSS estimates.

As discussed in the previous section, the KL transform can be used as a sparsifying transform. In this case, figure 2 should be changed accordingly to reflect that the $\boldsymbol{\rho}$ is no longer in the x–f domain. However, all the remaining reconstruction flowchart is exactly the same.

4. Experimental results

4.1. In vivo cardiac cine imaging

4.1.1. Methods. For *in vivo* experiments, we have acquired 25 frames of full k-space data from a cardiac cine of a patient using a 1.5 T Philips scanner at Yonsei University Medical Center. The field of view (FOV) was 345.00×270.00 mm^2, and the matrix size for scanning

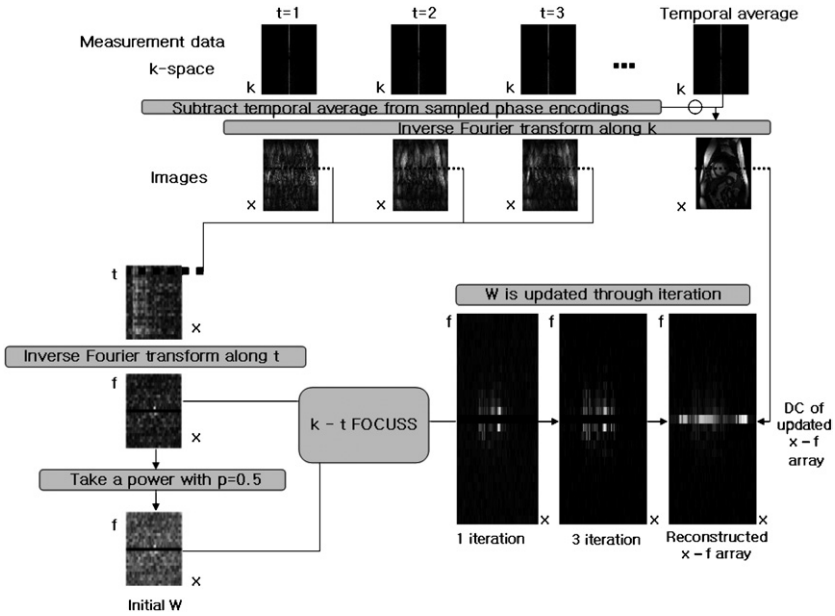

Figure 2. *k–t* FOCUSS reconstruction flow. In *k–t* FOCUSS, an estimate of the (x, f) support is updated with iterations.

was 256×220, which corresponds to 220 phase encoding steps and 256 samples in frequency encoding. In these experiments, the phase encoding direction is horizontal. The slice thickness was 10.0 mm, and the acquisition sequence was steady-state free precession (SSFP) with a flip angle of 50° and $T_R = 3.45$ ms. The heart frequency was 66 bpm, and retrospective cardiac gating was used. The magnitude image of this reconstructed *complex valued* cardiac cine from the full *k*-space samples is used as a ground-truth reference image to evaluate the reconstruction quality of *k–t* FOCUSS.

In the first simulation, we extracted 55 phase encodings from the full 220 phase encodings using the Gaussian random sampling pattern, which corresponds to the reduction factor of 4. Since the downsampling was done using *actual k*-space measurement data, no Hermitian symmetry was assumed. This allows us to evaluate the effects of phase variations during the MR acquisition. Additionally, we have tested our *k–t* FOCUSS algorithm from a higher reduction factor like $8\times$ or $16\times$ acceleration. Also, for these higher reduction factors, we apply the parallel imaging version of *k–t* FOCUSS to improve the results.

4.1.2. Results. We have analyzed the reconstruction performance of *k–t* FOCUSS with iterations. Since the downsampling is along the phase encoding direction, the aliasing patterns along the horizontal direction were observed when the cardiac cine was reconstructed using the zero-padded Fourier transform (see figure 3(b)). When our *k–t* FOCUSS algorithm is applied to these images, more iterations significantly improve the image quality, but after the fifth iteration, little improvement was observed, indicating that *k–t* FOCUSS has converged (see figures 4(c)–(d)). We have also illustrated the corresponding x–f supports in the right column of figures 3 and 4. The original x–f support is sparse. The estimated x–f support for the fifth iteration of *k–t* FOCUSS is sparse and clearly catches the significant part of the true x–f support. Additionally, we have also illustrated reconstruction results using the sliding

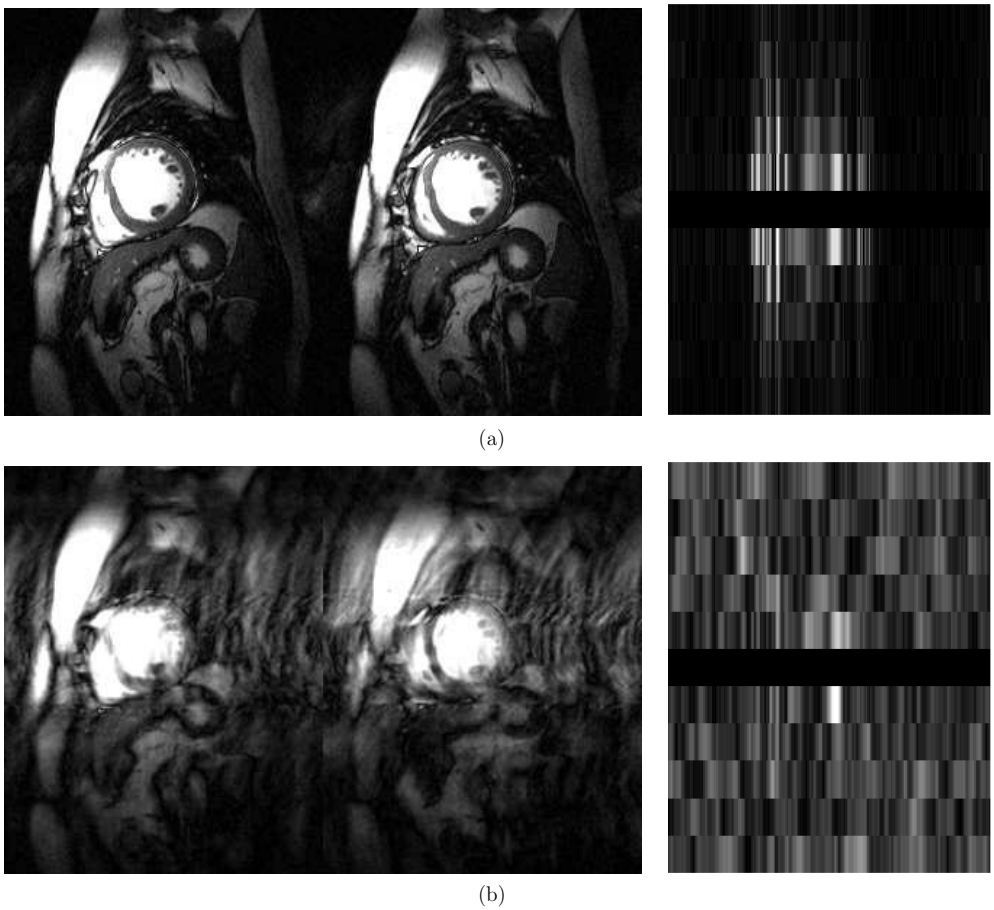

Figure 3. *In vivo* cardiac cine reconstructed from (a) full k-space samples, and (b) direct Fourier transform of zero-padded measurement data. The right-most column corresponds to the corresponding x–f supports. The acceleration factor for (b) is 4.

window method with the window size of four in figure 4(a). The sliding window method was implemented as follows. First, to fill out the missing k-space samples for each frame, the k-space data in neighboring frames were used. The window was centered on the current frame, and the nearest k-data from the current frame within the window were used to fill out the missing k-space samples on the current frame. After applying this procedure for every frame, we were able to reconstruct the time-varying image sequences. As shown in figure 4, our k–t FOCUSS results outperform it.

In order to show the difference clearly, we have calculated the difference images between the original cardiac cine and the reconstruction results from the down sampled data. Figure 5(a) shows the difference images between the original and reconstructed images from the sliding window methods using the window size four. The aliasing artifacts along the phase encoding direction are observed. Figure 5(b) shows the difference images between the original and the first iteration of k–t FOCUSS. Here, the artifacts are still strong along the phase encoding direction. We can also observe that the artifacts at the cardiac boundary are significant due to temporal blurring. However, at the fifth iteration of k–t FOCUSS, as shown in figure 5(c), the residual energy along the heart boundaries and aliasing artifacts along the

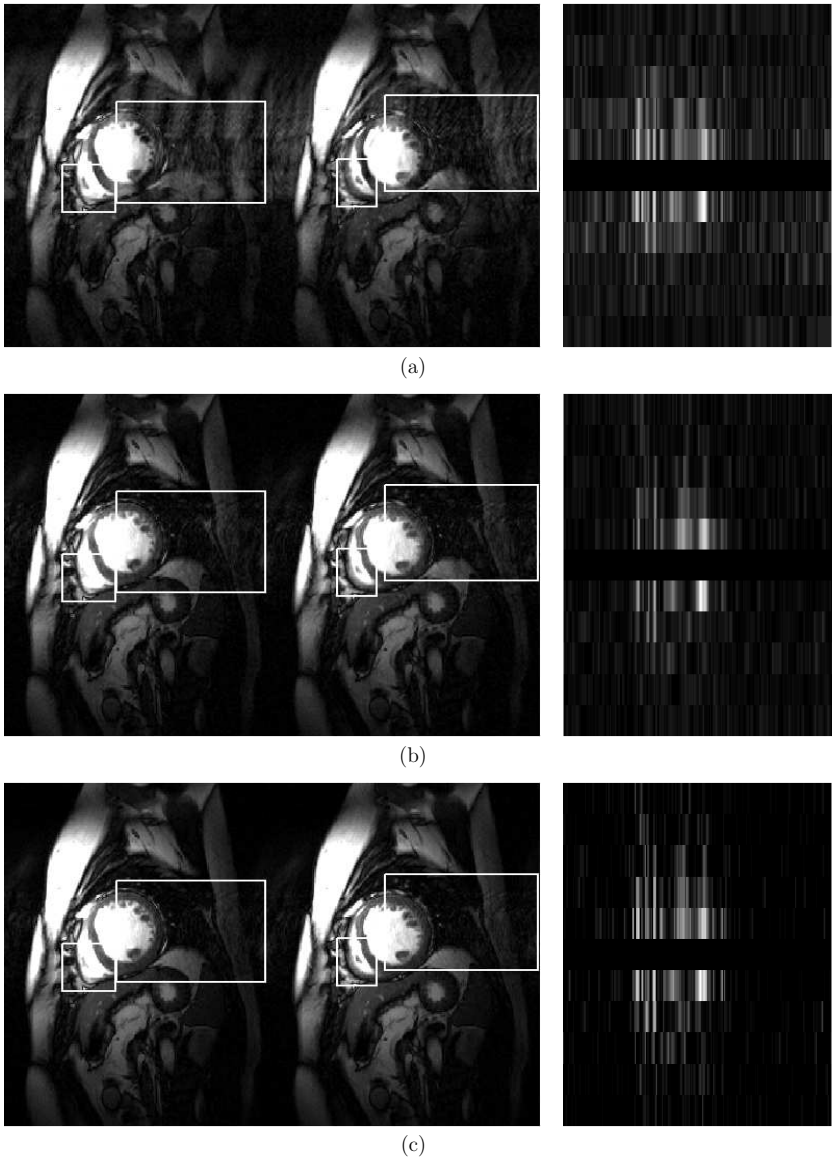

Figure 4. *In vivo* cardiac cine reconstructed from (a) the sliding window method with the window size of 4, (b) *k–t* FOCUSS with one iteration, and (c) *k–t* FOCUSS with five iterations, respectively. The highly improved parts are highlighted by white boxes. The right-most column corresponds to the corresponding x–f supports. The acceleration factor is 4.

phase encoding direction were mostly suppressed. To quantify the improvement, the frame-by-frame normalized MSE plots are calculated and illustrated in figure 6. The normalized MSE is defined by

$$\text{normalized MSE} = \frac{\|\boldsymbol{\rho} - \boldsymbol{\rho}_{\text{True}}\|_2^2}{\|\boldsymbol{\rho}_{\text{True}}\|_2^2} \tag{32}$$

where $\|\cdot\|_2$ denotes the L_2 norm and $\boldsymbol{\rho}$ and $\boldsymbol{\rho}_{\text{True}}$ represent the estimated and the true (x, f) images, respectively. Clearly, more iterations consistently reduce the MSE for all frames, and

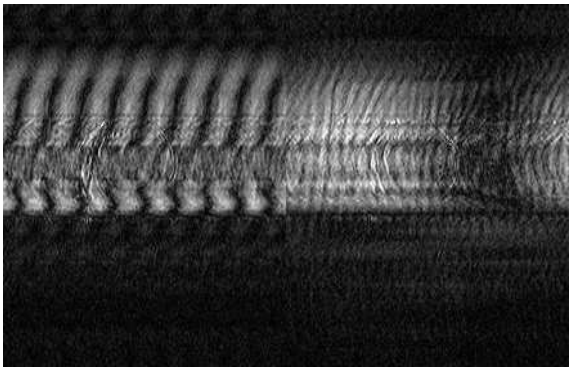

(a)

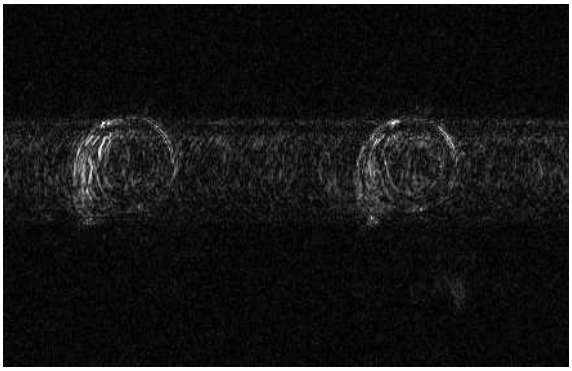

(b)

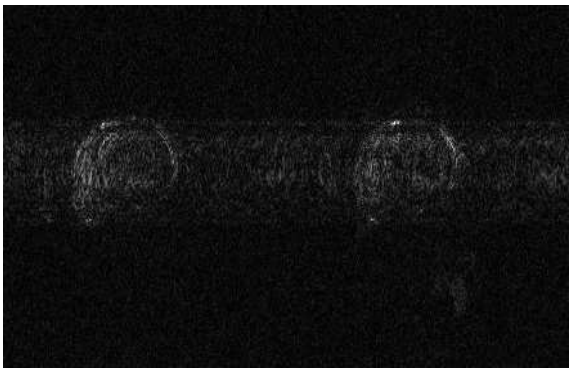

(c)

Figure 5. The difference images between the original cine images and reconstructions from (a) the sliding window method with the window size of 4, (b) *k–t* FOCUSS with one iteration, and (c) *k–t* FOCUSS with five iterations, respectively. The acceleration factor is 4.

the *k–t* FOCUSS results outperform that of the sliding window method with the window size of four.

Our *k–t* FOCUSS algorithm has been also applied for a higher acceleration factor. As shown in figure 7(a), excellent reconstruction quality was observed with 8-fold acceleration. However, for 16× acceleration, we started to see reconstruction artifacts over all the images (see figure 7(c)). However, these artifacts are efficiently suppressed using parallel coils (see

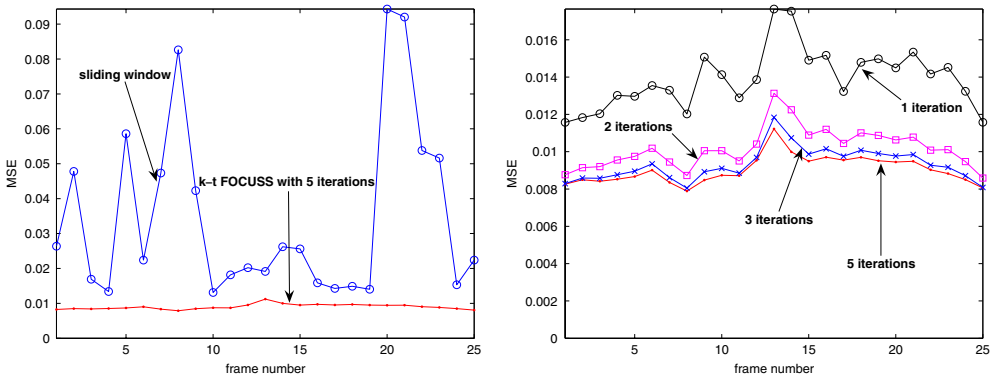

(a) (b)

Figure 6. The MSE plots of *k–t* FOCUSS for *in vivo* cardiac data with acceleration factor of 4. (a) Comparison between the sliding window and *k–t* FOCUSS, and (b) *k–t* FOCUSS results with respect to the number of iterations.

figures 7(b) and (d), respectively). In order to quantify these artifacts, we have also plotted an MSE for each time frame in figure 8. As expected, more iterations result in reconstruction quality improvements, and parallel coils reduce the reconstruction errors.

For comparison, we have also illustrated the conventional *k–t* BLAST results with a *lattice sampling pattern* in figures 9(a) and (b). Clearly, at the same acceleration factor, the wrap-around aliasing artifacts are observed in *k–t* BLAST reconstruction using a lattice sampling pattern. Of course, with the careful design of a lattice sampling pattern and sequence timing, the aliasing artifact in the *k–t* BLAST could be removed (Tsao *et al* 2003, 2005). However, our *k–t* FOCUSS is robust to sequence timing and *does not* need the careful design of a sampling pattern thanks to the power of the random sampling scheme.

4.2. fMRI experiments

4.2.1. Methods. The fMRI (functional MRI) is a technique that monitors brain hemodynamics. When a person is thinking or doing something, the nerve cells of his/her brain are activated by consuming oxygen in the blood. This phenomenon results in changes in the magnetic state of hemoglobin. As a consequence, we can detect a slightly different magnetic resonance signal of blood in the brain.

For the fMRI study, we designed a right finger tapping experiment using a block paradigm. The goal of this experiment was to figure out which part of the brain is activated when the right finger moves. We asked a subject to tap the right finger when a 'tap' sign appeared, and stop tapping when a 'stop' sign was presented. These tasks were periodically performed ten times. Each right finger tapping task was performed during 21 s, and the resting period between successive right finger tapping tasks was 30 s. Informed consent was obtained from each volunteer. *In vivo* brain data were acquired using a 3.0 T MRI system manufactured by ISOL Technology of Korea. A birdcage RF head coil was used for both the RF pulse transmission and the signal detection. We have acquired 184 frames with 3 s TR. The first 14 frames were obtained for calibration. From the 15th frame, every 17 frames show one block of the right finger tapping experiments. The acquisition sequence was EPI with a flip angle of 80°. We have obtained *k*-space data on a 64×64 matrix size. The number of slices was 35, and the thickness of each slice was 4 mm. Each voxel size was $3.4375 \times 3.4375 \times 4$ mm^3, so we could obtain a 220×220 mm^2 field of view. After we obtained the full *k*-space data, we used

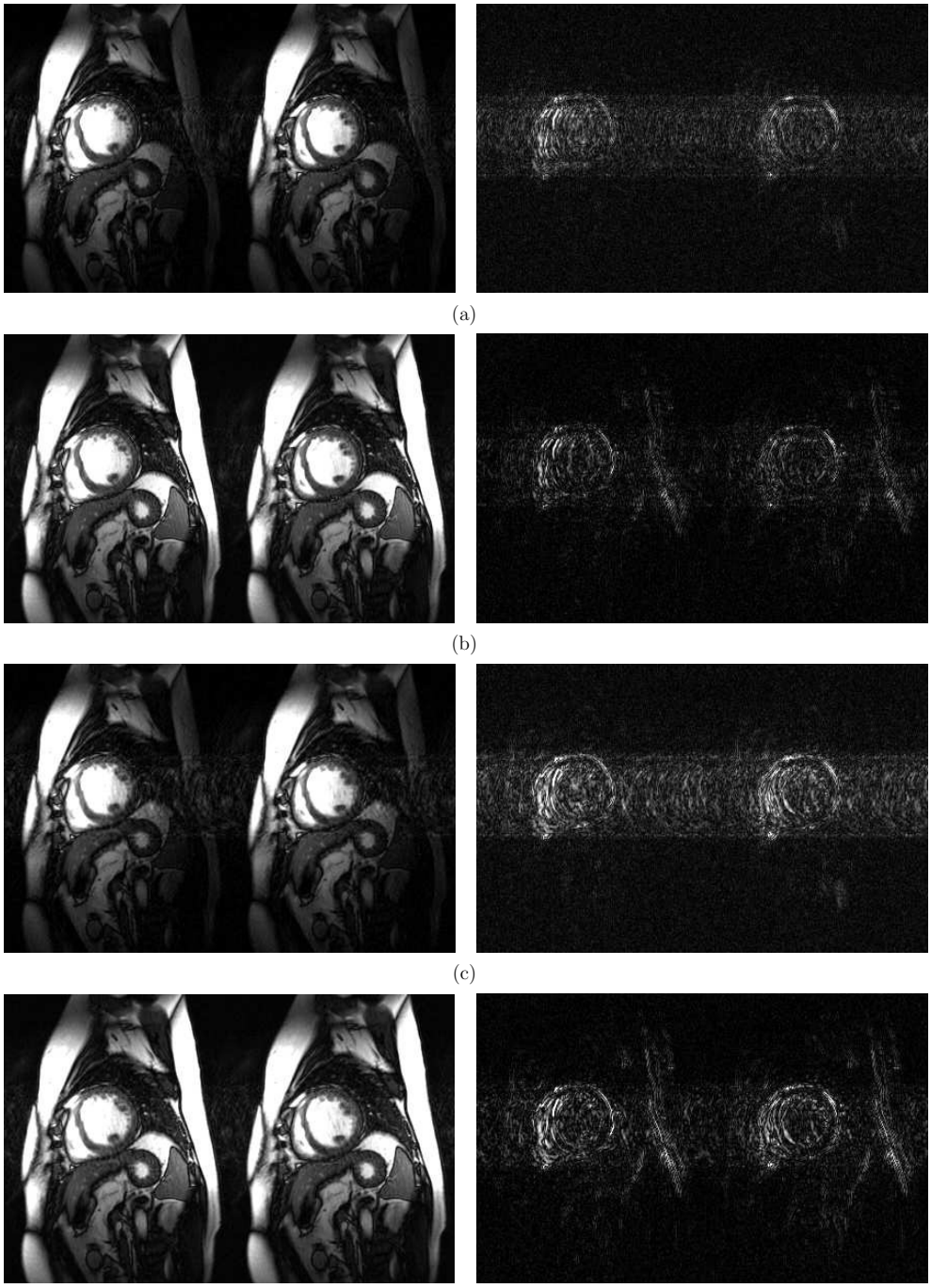

Figure 7. (a) Single coil *k–t* FOCUSS reconstruction results with 8× acceleration factor; (b) five coil parallel *k–t* FOCUSS reconstruction with 8× acceleration factor; (c) single coil *k–t* FOCUSS reconstruction with 16× acceleration factor; (d) five coil parallel *k–t* FOCUSS reconstruction with 16× acceleration factor. The right column shows the difference images between the original cine images and reconstructions.

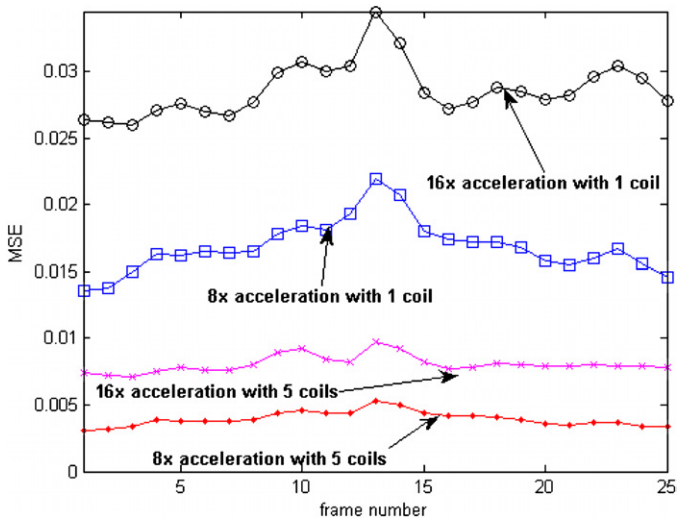

Figure 8. MSE plots of *k–t* FOCUSS with 16× acceleration factor for single and five coils, and with 8× acceleration factor for single and five coils, respectively.

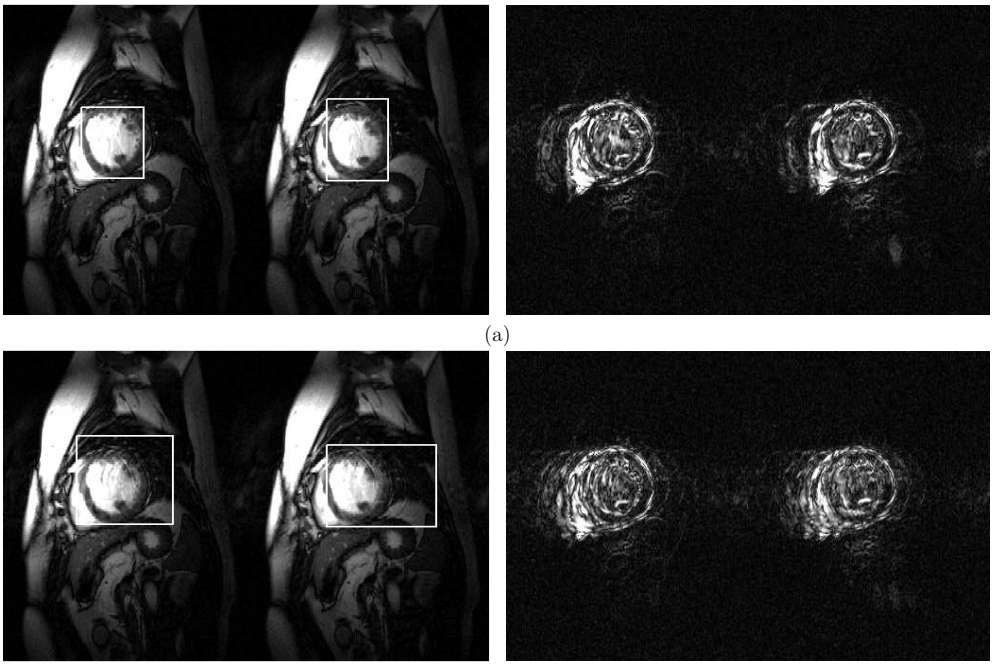

(a)

(b)

Figure 9. *k–t* BLAST for lattice sampling pattern from (a) 8-fold acceleration and (b) 16-fold acceleration. The aliasing artifacts are highlighted by white boxes. The right column shows the difference images between the original cine images and reconstructions.

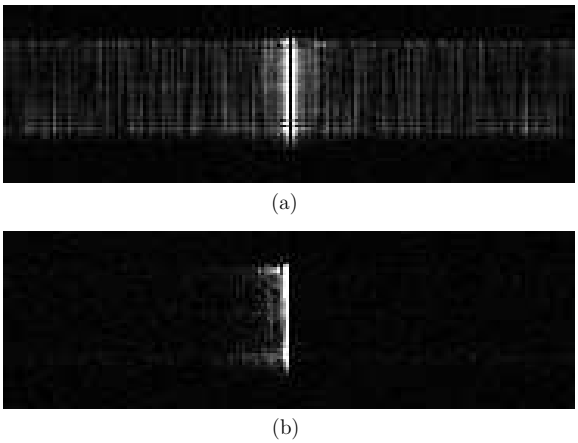

Figure 10. (a) x–f support obtained from fully sampled data; and (b) sparse signal support after the KL transform.

the SPM (statistical parametric mapping (Friston *et al* 1995)) toolbox on Matlab to analyze the activated parts during the right finger tapping. From the full k-space data, we applied random downsampling to obtain partial k-space data. The sampling pattern was similar to figure 1. Since the downsampled data were obtained directly from the complex valued k-space data, no Hermitian symmetry was assumed. By applying our k–t FOCUSS algorithm for each slice, we reconstructed aliasing free 3D brain image sequences. Here, we used a slightly different temporal transform method from the *in vivo* cardiac cine imaging experiment. As shown in figure 10(a), the original x–f support obtained from fully sampled data was spread over whole frequency, so we applied the KLT/PCA to make the signal much sparser. The principal components were calculated from low-resolution x–f support obtained using only low-frequency k-space samples. As shown in figure 10(b), the KLT/PCA significantly reduces the nonzero coefficients. To calculate the activated area and compare it with the reference model, the SPM toolbox was again used with exactly the same parameters as in the full data case for the reconstructed sequences.

4.2.2. Results. We have applied our k–t FOCUSS algorithm for the reduction factors of 8. A total of five k–t FOCUSS iterations were applied. Then, we used the SPM toolbox to analyze the activated area using the final k–t FOCUSS reconstruction results. In fact, the SPM detection of the activated area is calculated from the slight differences of the time-varying images. Even if we have already verified our algorithm using the cardiac cine, the main goal of the fMRI experiment is to additionally confirm that our k–t FOCUSS can catch even the slight differences hardly visible with the naked eye.

The reference and k–t FOCUSS reconstruction with $8\times$ downsampling are shown in figures 11(a) and (b), respectively. Visually similar results were obtained. Now, we use the SPM toolbox to calculate the activated area, as shown in figure 12(b) for reduction factors of 8. The result in figure 12(a) illustrates the activated detection part from the full k-space data, which confirms the fact that the left motor cortex is activated during right finger tapping. We used this result as a reference model to verify the performance of our algorithm for an fMRI study. We overlayed the activated area to the brain phantom, as shown in the right column of figure 12, using the SPM toolbox. The p-values for SPM analysis were 0.05 for all the experiments. Figure 12(b) illustrates the reconstruction results using our k–t FOCUSS

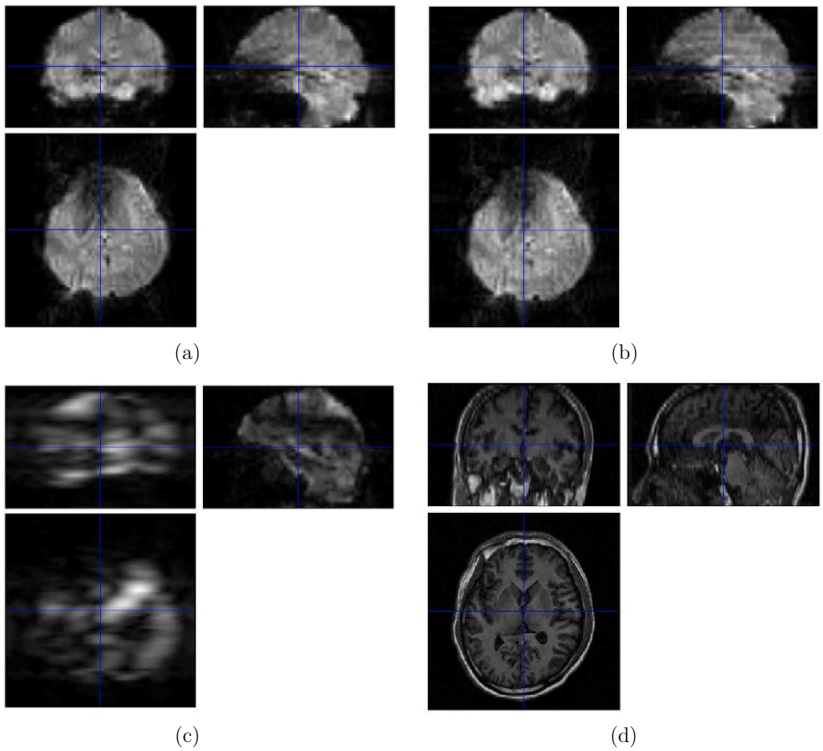

Figure 11. Reconstructed volumes using (a) fully sampled *k*-space data, (b) *k–t* FOCUSS at the 8-fold acceleration, and (c) low-frequency-only data at the 8-fold acceleration, respectively. The image size for each slice is 64 × 64. Figure (d) shows a T1 image of 256 × 256 size.

at the 8-fold downsampling factor. Compared to the results obtained from the fully sampled data, the activated areas in figure 12(b) are somewhat weaker, but the strongly activated parts are still correctly identified. Additionally, we also plotted the average time curve for the activated area in figure 13. We can see that the *k–t* FOCUSS results follow that of the full data reference, as illustrated in figure 13. To confirm the performance improvement of *k–t* FOCUSS over conventional processing, we generated the reconstruction results using only the eight lowest *k*-space frequency samples (i.e. 8-fold acceleration) in figure 12(c), which clearly shows the blurred map of the activated area and even indicates activation outside of the brain. Furthermore, by comparing figures 11(b) and (c), we clearly see that our *k–t* FOCUSS algorithm shows very clear reconstruction results, even from very limited data samples.

So far, small EPI matrix sizes were unavoidable for fMRI analysis to keep the temporal resolution and to obtain time-varying images without aliasing. As shown in figures 11(a)–(c), the reconstructed image size is usually 64 × 64. Since this size is too small to show the accurate coordinate of the activated area on the brain, we need to up-sample the reconstructed images to a much larger size. To map the small size image to a larger size, a T1 image is used as a large reference brain image, as shown in figure 11(d). In our experiment, a T1 image of 256 × 256 size was acquired before the right finger tapping task. As a consequence, artifacts are unavoidable during the registration with the high-resolution T1 images. However, the *k–t* FOCUSS algorithm could allow a larger image size during the same T_R without aliasing artifacts. Hence, we expect that *k–t* FOCUSS might be a valuable tool for high-resolution fMRI.

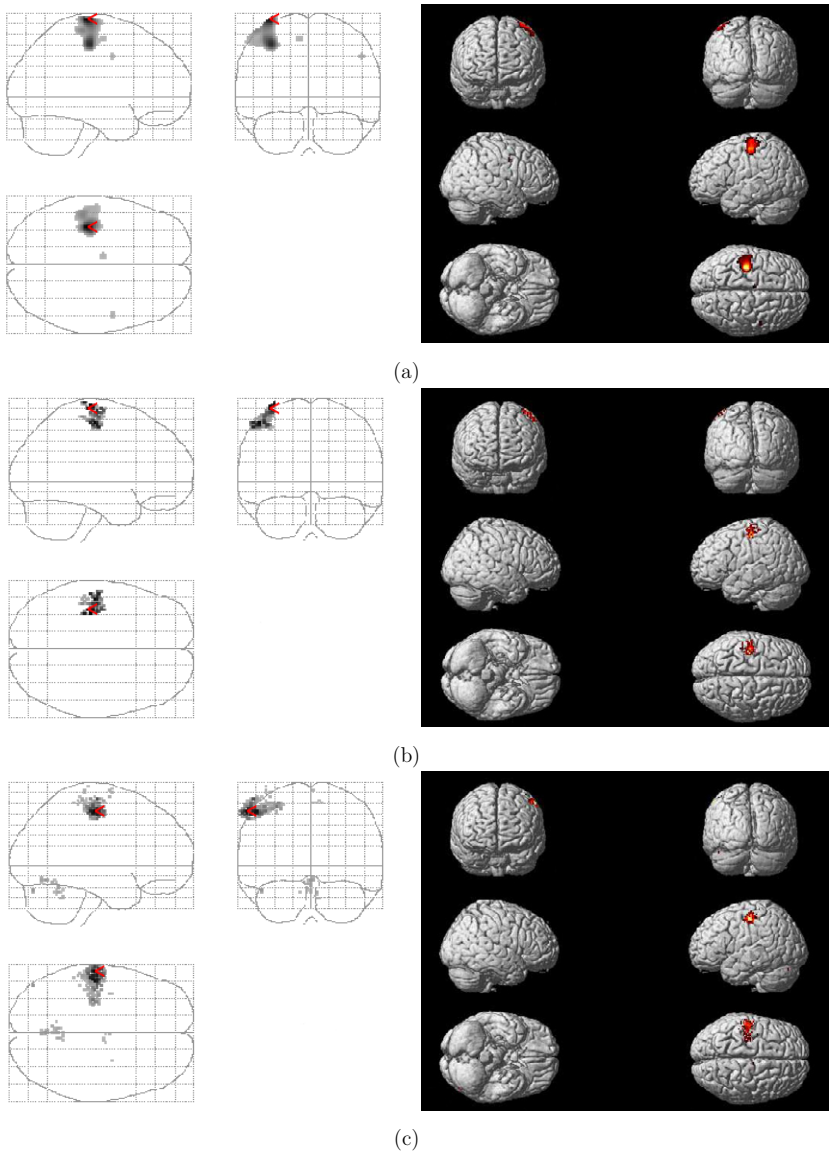

Figure 12. The fMRI results for right finger tapping experiment. The activated areas are calculated using the SPM toolbox from the reconstruction results using (a) original fully sampled data, (b) *k–t* FOCUSS reconstruction at the 8-fold acceleration, and (c) low-frequency data at the 8-fold acceleration, respectively.

5. Discussion

5.1. Hyper parameter setting

There are multiple hyper parameters that affect the performance of the *k–t* FOCUSS, such as the regularization factor λ in equation (17), the power factor p in equation (15), and the number of iterations. The parameter λ controls the stability of the solution under noisy conditions.

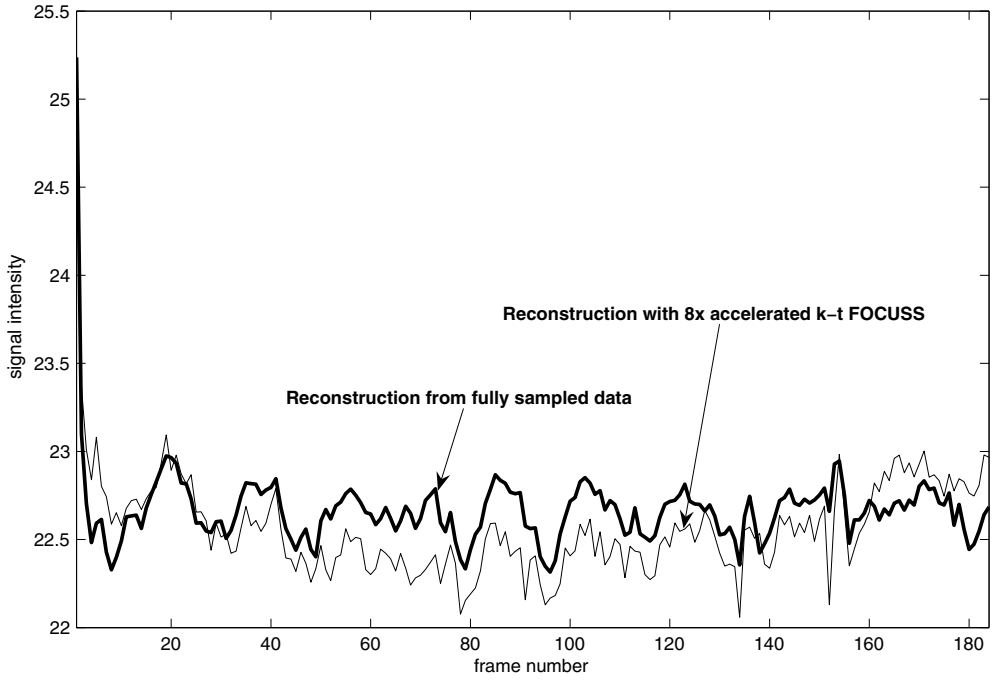

Figure 13. Time curve for the right finger tapping experiments.

Figure 14 shows the reconstruction results from *k–t* samples from a low signal-to-noise ratio (SNR) body coil with various λ. For a small λ, the *k–t* FOCUSS reconstruction results become noisier. On the other hand, for an appropriately large λ, the noise pattern disappears while the reconstruction becomes slightly smoothed out. For most of the high-quality *k–t* measurements from a real scanner, we found that $\lambda = 0.1$ performs best.

Figures 15(a) and (b) illustrate the effects of the power factor p. If p approaches 1, the solution becomes more sparse and only strong frequency features are reconstructed, resulting in visually annoying artifacts, as shown in figure 15(a). Figure 15(b) is the reconstruction results with $p = 0.5$, which is the best in reconstruction quality.

5.2. Lattice sampling pattern

Similar to *k–t* BLAST using a lattice sampling pattern, the computational complexity of *k–t* FOCUSS could be greatly reduced if the (k, t) samples were obtained on the lattice. More specifically, let us define a two-dimensional lattice Λ as

$$\Lambda = \{n_1\mathbf{v}_1 + n_2\mathbf{v}_2 : n_1, n_2 \in \mathbb{Z}\} \tag{33}$$

where $\mathbf{v}_1$ and $\mathbf{v}_2$ are linearly independent vectors and n_1, n_2 are integers. Here, $\mathbf{V} = [\mathbf{v}_1, \mathbf{v}_2]$ denotes the sampling matrix or basis matrix, and the sampling density is defined by $1/d(\mathbf{V})$, where $d(\mathbf{V})$ denotes the determinant of matrix $\mathbf{V}$. The reciprocal lattice Λ^* is then defined as the lattice that has the basis matrix $\mathbf{V}^* = \mathbf{V}^{-T}$, where $\mathbf{V}^{-T}$ denotes the transpose of the inverse of $\mathbf{V}$.

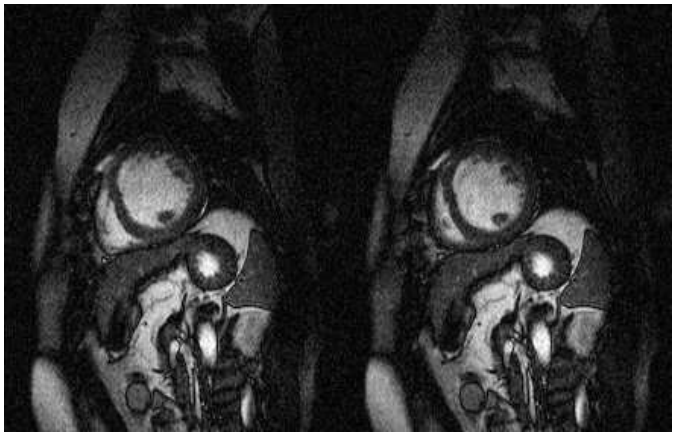

(a)

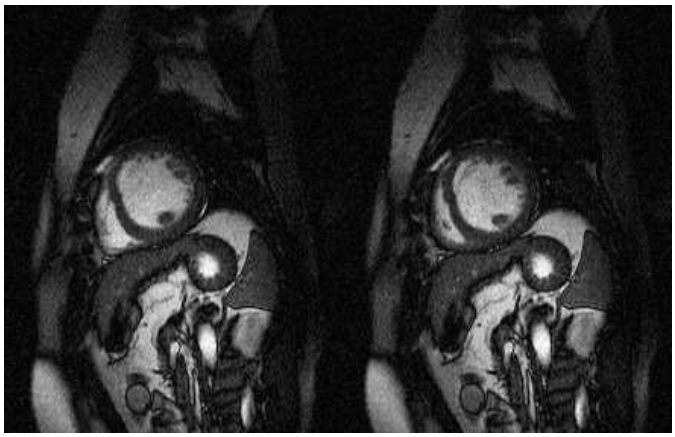

(b)

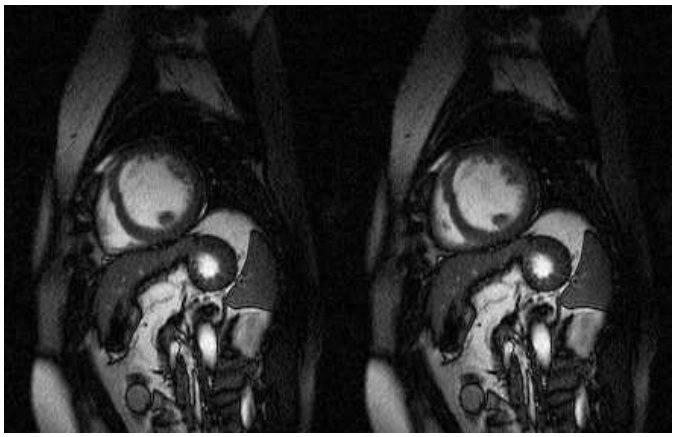

(c)

Figure 14. *k–t* FOCUSS reconstruction for 4× reduction from noisy measurements with (a) $\lambda = 0$, (b) $\lambda = 100$ and (c) $\lambda = 500$ respectively. These results are obtained after five iterations.

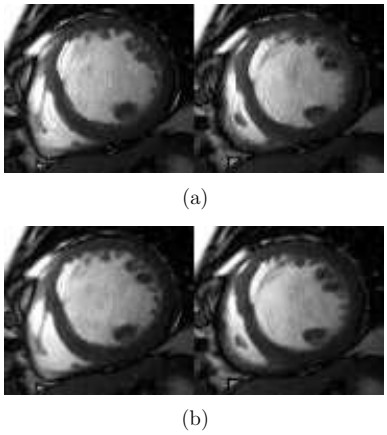

(a)

(b)

Figure 15. *k–t* FOCUSS reconstruction for 4× reduction with (a) $p = 1$, and (b) $p = 0.5$. These results are obtained after five iterations.

Suppose that the continuous signal $\upsilon(k, t)$ is sampled on lattice Λ. Then, the corresponding 2D Fourier transform $\theta(x, f)$ of the sampled $\upsilon(k, t)$ is composed of replicas on the reciprocal lattice Λ^* (Dubois 1985):

$$\theta\left(\begin{bmatrix} x \\ f \end{bmatrix}\right) = \frac{1}{d(\mathbf{V})} \sum_{n_1, n_2} \rho\left(\begin{bmatrix} x \\ f \end{bmatrix} - \mathbf{V}^{-T} \begin{bmatrix} n_1 \\ n_2 \end{bmatrix}\right). \tag{34}$$

In operator form, equation (34) can be written as

$$\boldsymbol{\theta} = \mathbf{M}\boldsymbol{\rho} \tag{35}$$

where $\mathbf{M}$ denotes the overlap index operator, whose (i, j) elements are 1 if contribution exists from the jth original (x, f)-pixel to the ith *aliased* (x, f) pixel; otherwise it is zero. Then, our *k–t* FOCUSS update equation for equation (35) can be simplified by

$$\boldsymbol{\rho}_n = \boldsymbol{\Theta}_n \mathbf{M}^H (\mathbf{M}\boldsymbol{\Theta}_n \mathbf{M}^H + \lambda \mathbf{I})^{-1} \boldsymbol{\theta} \tag{36}$$

or in another offset form

$$\boldsymbol{\rho}_n = \bar{\boldsymbol{\rho}} + \boldsymbol{\Theta}_n \mathbf{M}^H (\mathbf{M}\boldsymbol{\Theta}_n \mathbf{M}^H + \lambda \mathbf{I})^{-1} (\boldsymbol{\theta} - \mathbf{M}\bar{\boldsymbol{\rho}}). \tag{37}$$

Due to the special structure of the overlap index matrix $\mathbf{M}$, equations (36) and (37) can be decomposed into a pixel-by-pixel update in the (x, f) space (Tsao *et al* 2003).

However, the main weakness of such a modification of *k–t* FOCUSS is that the lattice sampling pattern does not satisfy the assumption for the compressed sensing theory (Donoho 2006). Hence, we can easily expect that the advantage of the *k–t* FOCUSS over *k–t* BLAST/SENSE should not be significant in the lattice sampling pattern compared to the random sampling pattern.

5.3. Computational complexity

As discussed above, *k–t* FOCUSS is more effective for a random sampling pattern rather than a lattice sampling pattern. However, for the random sampling pattern, the main drawback of *k–t* FOCUSS is the computational burden. Note that the computational burden for *k–t* FOCUSS comes from the matrix inversion in equations (16) and (17).

In order to reduce the computational burden of *k–t* FOCUSS, the matrix inversion is skipped by using a conjugate gradient (CG) method (Chong and Zak 1996). In CG, the most important step is the calculation of the gradient. The gradient of the cost function equation (12) with respect to $\mathbf{q}$ is given by

$$\frac{\partial C(\mathbf{q})}{\partial \mathbf{q}} = -\mathbf{W}_n^H \mathbf{F}^H (\upsilon - \mathbf{F}\bar{\rho} - \mathbf{F}\mathbf{W}\rho) + \lambda \mathbf{q} \tag{38}$$

which can be decomposed into the following consecutive steps:

weighting:	$\mathbf{W}\mathbf{q}$	(39)
2D Fourier transform:	$\mathbf{F}\mathbf{W}\mathbf{q}$	(40)
substraction:	$\upsilon - \mathbf{F}\bar{\rho} - \mathbf{F}\mathbf{W}\mathbf{q}$	(41)
2D inverse Fourier transform:	$\mathbf{F}^H(\upsilon - \mathbf{F}\bar{\rho} - \mathbf{F}\mathbf{W}\mathbf{q})$	(42)
weighting and sum:	$-\mathbf{W}^H\mathbf{F}^H(\upsilon - \mathbf{F}\bar{\rho} - \mathbf{F}\mathbf{W}\mathbf{q}) + \lambda\mathbf{q}$	(43)

since the inverse Fourier transform is the adjoint of the fast Fourier transform. The main computational burden comes from equations (40) and (42). The fast Fourier transform (FFT), however, may significantly relieve the computational burden of these steps. In our *in vivo* cardiac experiment, the total 3D matrix size to be reconstructed was $220 \times 256 \times 25$. Using Matlab 7.0.4 on a Xeon 3 GHz with 2 GB RAM, it took 100 s to reconstruct the final cardiac cine using our *k–t* FOCUSS algorithm with five iterations.

6. Conclusion

Using a random *k–t* sampling pattern and FOCUSS algorithm, we designed a new dynamic imaging algorithm called *k–t* FOCUSS, which is asymptotically optimal from the compressed sensing theory and encompasses the celebrated *k–t* BLAST and *k–t* SENSE as special cases. Our *k–t* FOCUSS does not require a training phase or *a priori* knowledge of the *x–f* support. Furthermore, thanks to the random sampling pattern, our *k–t* FOCUSS is robust and insensitive to the sequence timing. We have applied our *k–t* FOCUSS to dynamic MR imaging problems, such as cardiac cine and fMRI experiments and obtained highly improved reconstruction from severely downsampled *k*-space data.

Despite the surprising performance of *k–t* BLAST and *k–t* SENSE, a theoretical explanation for their algorithm was not sufficient. Our analysis showed that *k–t* BLAST/SENSE is indeed the first iteration of our *k–t* FOCUSS algorithm and the diagonal covariance matrix in *k–t* BLAST/SENSE is actually the reweighted matrix updated from the initial low-resolution estimate. We expect that the insight we have acquired from the development of *k–t* FOCUSS not only improves the quality of *k–t* BLAST and *k–t* SENSE, but also opens a new area of research.

Acknowledgments

This research was supported in part by a Brain Neuroinformatics Research program by the Korean Ministry of Commerce, Industry, and Energy, and in part by grant no. 2004-020-12 from the Korea Ministry of Science and Technology (MOST). The authors would like to thank Dr Byung Wook Choi at Yonsei Medical Center for various discussions.

References

Aggarwal N, Zhao Q and Bresler Y 2002 Spatio-temporal modeling and minimum redundancy adaptive acquisition in dynamic MRI *Proc. 1st IEEE Int.Symp. Biomed. Imaging ISBI-2002,* pp 737–40

Candes E, Romberg J and Tao T 2006a Robust uncertainty principles: exact signal reconstruction from highly incomplete frequency information *IEEE Trans. Inf. Theory* **52** 489–509

Candes E, Romberg J and Tao T 2006b Stable signal recovery from incomplete and inaccurate measurements *Commun. Pure Appl. Math.* **59** 1207–33

Candes E and Tao T 2005 Decoding by linear programming *IEEE Trans. Inf. Theory* **51** 4203–15

Carr H Y 1958 Steady-state free precession in nuclear magnetic resonance *Phys. Rev.* **112** 1693–701

Chong E K P and Zak S H 1996 *An Introduction to Optimization* (New York: Wiley-Interscience)

Donoho D L 2006 Compressed sensing *IEEE Trans. Inf. Theory* **52** 1289–306

Dubois E 1985 Sampling and reconstruction of time-varying imagery with application in video systems *Proc. IEEE* **73** 502–22

Friston K J, Holmes A P, Worsley K J, Poline J-P, Frith C D and Frackowiak R S J 1995 Statistical parametric maps in functional imaging: a general linear approach *Human Brain Mapp.* **2** 189–210

Gorodnitsky I F, George J S and Rao B D 1995 Neuromagnetic source imaging with FOCUSS: a recursive weighted minimum norm algorithm *Electroencephalogr. Clin. Neurophysiol.* **95** 231–51

Gorodnitsky I F and Rao B D 1997 Sparse signal reconstruction from limited data using FOCUSS: re-weighted minimum norm algorithm *IEEE Trans. Signal Process.* **45** 600–16

Griswold M A, Jakob P M, Heidemann R M, Nittka M, Jellus V, Wang J, Kiefer B and Haase A 2002 Generalized autocalibrating partially parallel acquisitions (GRAPPA) *Magn. Reson. Med.* **47** 1202–10

Griswold M A, Jakob P M, Nittka M, Goldfarb J W and Haase A 2000 Partially parallel imaging with localized sensitivities (PILS) *Magn. Reson. Med.* **44** 602–9

Hansen M S, Kozerke S, Pruessman K P, Boesiger P, Pedersen E M and Tsao J 2004 One the influence of training data quality in *k–t* BLAST reconstruction *Magn. Reson. Med.* **52** 1175–83

Haupt J and Nowak R 2006 Signal reconstruction from noisy random projections *IEEE Trans. Inf. Theory* **52** 4036–48

Kellman P, Epstein F H and McVeigh E R 2001 Adaptive sensitivity encoding incorporating temporal filtering (TSENSE) *Magn. Reson. Med.* **45** 846–52

Kim J, Jong C Y and Yoo J 2006 *x–f* SENSE: optimal spatio-temporal sensitivity encoding for dynamic MR imaging *Proc. IEEE Int. Symp. Biomed. Imaging ISBI-2006 (Arlington, VA)*

Kozerke S, Tsao J, Razavi Reza and Boesiger P 2004 Accelerating cardiac cine 3D imaging using *k–t* BLAST *Magn. Reson. Med* **52** 19–26

Kreutz-Delgado K, Murray J F, Rao B D, Engan K, Lee T W and Sejnowski T J 2003 Dictionary learning algorithms for sparse representation *Neural Comput.* **15** 349–96

Lee V S 2005 *Cardiovascular MRI: Physical Principles to Practical Protocols* (Philadelphia, PA: Lippincott Williams & Wilkins)

Lustig M, Santos J M, Donoho D L and Pauly J M 2006a *k–t* SPARSE: high frame rate dynamic MRI exploiting spatio-temporal sparsity *Proc. ISMRM (Seattle, WA)*

Lustig M, Donoho D L and Pauly J M 2006b Rapid MR imaging with compressed sensing and randomly under-sampled 3DFT trajectories *Proc. ISMRM (Seattle, WA)*

Madore B, Glover G H and Pelc N J 1999 Unaliasing by Fourier-encoding the overlaps using the temporal dimension(UNFOLD), applied to cardiac imaging and fMRI *Magn. Reson. Med.* **42** 813–28

Plein S, Bloomer T N, Ridgway J P, Jones T R, Bainbridge G J and Sivananthan M U 2001 Steady-state free precession magnetic resonance imaging of the heart: comparison with segmented *k*-space gradient-echo imaging *J. Magn. Reson. Imaging* **14** 230–6

Poor H V 1994 *An Introduction to Signal Detection and Estimation* 2nd edn (New York: Springer)

Portniaguine O, Bonifasi C, DiBella E and Whitaker R 2003 Inverse methods for reduced *k*-space acquisition *Proc. ISMRM (Toronto, Canada)* p 481

Pruessmann K P, Weigher M, Scheidegger M B and Boesiger P 1999 SENSE: Sensitivity encoding for fast MRI *Magn. Reson. Med.* **42** 952–62

Sharif B and Bresler Y 2006 Optimal multi-channel time-sequential acquisition in dynamic MRI with parallel coils *Proc. IEEE Int. Symp. Biomed. Imaging ISBI-2006 (Arlington, VA)*

Sodickwon D K and Manning W J 1997 Simultaneous acquisition of spatial harmonics (SMASH): fast imaging with radiofrequency coil arrays *Magn. Reson. Med.* **38** 591–603

Stehling M K, Turner R and Mansfield P 1991 Echo-planar imaging: magnetic resonance imaging in a fraction of a second *Science* **254** 43–50

Tsao J 2002 On the UNFOLD method *Magn. Reson. Med.* **47** 202–7

Tsao J, Boesiger P and Pruessmann K P 2003 *K–t* BLAST and *k–t* SENSE: Dynamic MRI with high frame rate exploiting spatiotemporal correlations *Magn. Reson. Med.* **50** 1031–42

Tsao J, Kozerke S, Boesiger P and Pruessmann K P 2005 Optimizing spatiotemporal sampling for *k–t* BLAST and *k–t* SENSE: application to high-resolution real-time cardiac steady-state free precession *Magn. Reson. Med* **53** 1372–82

Willis N P and Bresler Y 1995 Optimal scan for time-varying tomography: II. Efficient design and experimental validation *IEEE Trans. Image Process.* **4** 654–66